NeuroImage 55 (2011) 468–478

Contents lists available at ScienceDirect

NeuroImage

journal homepage: www.elsevier.com/locate/ynimg

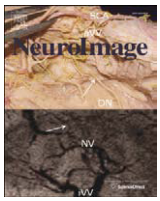

Age-associated reductions in cerebral blood flow are independent from regional atrophy

J. Jean Chen [a,b,*], H. Diana Rosas [a,c], David H. Salat [a,b,d]

[a] MGH/MIT/HMS Athinoula A. Martinos Center for Biomedical Imaging, Massachusetts General Hospital, Harvard Medical School, USA
[b] Department of Radiology, Massachusetts General Hospital, Harvard Medical School, USA
[c] Department of Neurology, Massachusetts General Hospital, Harvard Medical School, USA
[d] Neuroimaging Research for Veterans Center, VA Boston Healthcare System, USA

ARTICLE INFO

Article history:
Received 19 July 2010
Revised 7 December 2010
Accepted 9 December 2010
Available online 16 December 2010

Keywords:
Cerebral blood flow (CBF)
Aging
Arterial-spin labelling (ASL)
Magnetic resonance imaging (MRI)
Quantitative perfusion
Alzheimer's disease
Dementia
Cortical thickness
Cerebral cortex

ABSTRACT

Prior studies have demonstrated decreasing cerebral blood flow (CBF) in normal aging, but the full spatial pattern and potential mechanism of changes in CBF remain to be elucidated. Specifically, existing data have not been entirely consistent regarding the spatial distribution of such changes, potentially a result of neglecting the effect of age-related tissue atrophy in CBF measurements. In this work, we use pulsed arterial-spin labelling to quantify regional CBF in 86 cognitively and physically healthy adults, aged 23 to 88 years. Surface-based analyses were utilized to map regional decline in CBF and cortical thickness with advancing age, and to examine the spatial associations and dissociations between these metrics. Our results demonstrate regionally selective age-related reductions in cortical perfusion, involving the superior-frontal, orbito-frontal, superior-parietal, middle-inferior temporal, insular, precuneus, supramarginal, lateral-occipital and cingulate regions, while subcortical CBF was relatively preserved in aging. Regional effects of age on CBF differed from that of grey-matter atrophy. In addition, the pattern of CBF associations with age displays an interesting similarity with the default-mode network. These findings demonstrate the dissociation between regional CBF and structural alterations specific to normal aging, and augment our understanding of mechanisms of pathology in older adults.

Introduction

Continuous and sufficient cerebral blood flow (CBF) is vital to neural function; thus, cerebral perfusion, typically quantified by measuring the volume of blood passing through the microvascular network in a given volume of tissue over a certain duration, is a key indicator of cerebral health. It has long been established that CBF is normally coupled to cerebral oxygen ($CMRO_2$) and glucose consumption in steady state (Hoge et al., 1999; Sokoloff et al., 1977). Disruption of this system may suggest compromised vascular function and/or abnormal metabolism. It is therefore not surprising that reduced CBF and disrupted neurovascular coupling are associated with numerous pathological conditions, such as hypertension, ischemic stroke, and Alzheimer's disease (Girouard and Iadecola, 2006; Gsell et al., 2000). However, it is not fully understood if changes in CBF arise in normal aging, and whether such changes are associated with the well described tissue atrophy in older adults.

The brain undergoes a wide array of anatomical and functional changes in normal aging (Morrison and Hof, 1997), associated with an increasing risk of age-related neurovascular diseases that compromise the functional integrity of the neurological system. A number of epidemiological (Aguero-Torres et al., 2006; Breteler, 2000; Ruitenberg et al., 2005), pharmacotherapeutic (Duron and Hanon, 2010; Forette et al., 2002; Tzourio et al., 2003), and neuroimaging studies (Alsop et al., 2008; Dai et al., 2008c, 2009; Uh et al., 2010) suggest vascular contributions to Alzheimer's disease (AD) and other dementia (Bell and Zlokovic, 2009; Caroli et al., 2007; de la Torre, 2005; Dickstein et al., 2010; Helzner et al., 2009; Ruitenberg et al., 2005; Sachdev et al., 1999; Zlokovic, 2005). Thus, understanding changes in blood flow in cognitively healthy older adults is an important step towards differentiating normal from abnormal alterations in physiology (Elias et al., 1995; Farmer et al., 1990; Nagata et al., 2000; Skoog et al., 1996). Regional hypoperfusion has been found to be associated with amyloid accumulation (Driscoll et al., 2010; Sojkova et al., 2008) as well as cognitive deficits (Alves and Busatto, 2006). The reported links between perfusion reduction, neuronal damage and structural deterioration (Fierstra et al., 2010; Tohgi et al., 1998) beg the question of how aging-associated CBF reductions relate to the wide-spread cerebral atrophy (Akiyama et al., 1997; Buckner et al., 2004; Raz et al., 1997; Salat et al., 2004), and more critically, which changes are not secondary to normal aging but may instead indicate impending pathology. Invaluable clues can be gleaned by integrating quantitative perfusion and anatomical imaging.

* Corresponding author. A. A. Martinos Center for Biomedical Imaging, 149 13th Street Room 2301, Massachusetts General Hospital, Harvard Medical School, Charlestown, MA 02129, USA. Fax: + 1 617 726 1227.
E-mail address: jjchen@nmr.mgh.harvard.edu (J.J. Chen).

1053-8119/$ – see front matter © 2010 Elsevier Inc. All rights reserved.
doi:10.1016/j.neuroimage.2010.12.032

Perfusion imaging has conventionally been performed using positron-emission tomography (PET) (Beason-Held et al., 2009; Meltzer et al., 2000; Pantano et al., 1984), single-photon emission computed tomography (SPECT) (Alves and Busatto, 2006; Inoue et al., 2005; Yang et al., 2002), X-ray computed tomography (CT) (Akiyama et al., 1997; Meyer et al., 1994) and contrast-enhanced MRI (Helenius et al., 2003). Arterial-spin labelling (ASL) (Detre et al., 1998a,b; Oguz et al., 2003; Parkes et al., 2004; Williams et al., 1992; Wong et al., 1997) is a relatively novel and minimally invasive perfusion methodology requiring no exogenous tracers, and continuous ASL (CASL) (Detre et al., 1992, 1994, 1998a,b) as well as the more novel pseudo-continuous ASL (Dai et al., 2008b; Silva and Kim, 1999) have recently found application in clinical populations (Alsop et al., 2008, 2010; Detre et al., 1998a,b; Xu et al., 2010). However, regional CBF changes in cognitively healthy adults specific to the full adult life-span remains to be clarified. In this work, we examine the effects of normal adult aging on CBF using advanced anatomical models and morphological procedures which permitted the assessment of regional alterations in cortical and subcortical tissue. We used pulsed ASL in conjunction with high-resolution structural MRI to evaluate regional cortical and subcortical resting CBF measures in cognitively healthy older adults. Unique to this study is the mapping of MRI measurements of age-associations in CBF in relation to regional brain atrophy in a cortical surface-oriented manner. This procedure permitted detailed examination of the association between age-related changes in CBF and tissue volume, as well as the reduction of the potential influence of partial volume contamination on the CBF values. We found that reductions in CBF were independent of concurrent age-related tissue volume reduction, as perfusion can remain unaltered in regions of significant tissue atrophy. This apparent "dissociation" suggests that tissue shrinkage and hypoperfusion may not take place concurrently. Our findings underscore the importance of perfusion and structural measures as individually unique metrics of neurological changes in aging.

Materials and methods

Participants

This study involved 86 cognitively healthy participants, (38 men/48 women), aged from 22.9 to 88.2 years. These were subdivided into young (YA, age<40), middle-aged (MA, 40≤age<60) and older (OA, age≥60) adult groups. Younger adults were recruited through the MGH and local community, and older adults were recruited through the Harvard Cooperative Program on Aging (http://www.hebrewrehab.org/home_institute.cfm?id=90) and the Nurses' Health Study (http://www.channing.harvard.edu/nhs/) at Harvard Medical School and Brigham and Women's Hospital as well as the local community. Older adults were screened for dementia using the Mini Mental Status Exam (MMSE) (Folstein et al., 1975), with a minimum MMSE requirement of 24. We also included scores from the National Adult Reading Test (ANART) (Grober and Silwinski, 1991) and the Hopkins Verbal Learning Test (HVLT) (Vanderploeg et al., 2000) as indicators of cognitive health, as well as the Geriatric Depression Scale (GDS) for psychiatric health (Yesavage et al., 1982). Demographic information is provided in Table 1. Education levels were matched in all age groups. We excluded individuals with signs of major neurologic or psychiatric illnesses outside the range of vascular conditions in our inclusion criteria (mild forms of hypertension, hyperlipidemia, and diabetes). History of diabetes or high blood pressure was noted. Conditions for exclusion included dementia, high cerebrovascular disease risk, cancer of the central nervous system, major head trauma, overt cerebrovascular disease (including stroke and hemorrhage), and other neurological or psychiatric conditions that would be expected to influence cognition or imaging measures including human immunodeficiency infection (HIV), hydrocephalus, brain tumors, sarcoidosis, and multiple sclerosis. We also excluded individuals taking medications that would be expected to have a substantial effect on cognitive abilities. Experiments were performed with the understanding and written consent of each participant, according to the Institutional Review Board guidelines.

Table 1
Demographics for young (YA), middle-aged (MA) and older (OA) participants (*MMSE*: Mini-mental Mental Status Exam; *ANART*: National Adult Reading Test; *HVLT*: Hopkins Verbal Learning Test (HVLT); *GDS*: Geriatric Depression Scale; *TRAILS-A&B*: Trail-making Tests A and B).

(a)

Group	*N*	Age [years]			ANART	Education [years]
		All	Men	Women		
YA	11 (5 M/6 F)	30.1 ± 6.4	29.3 ± 5.3	30.8 ± 5.6	12.5 ± 8.2	16.1 ± 1.1
MA	38 (16 M/22 F)	52.0 ± 5.9	51.1 ± 6.3	52.9 ± 5.3	11.8 ± 7.6	16.5 ± 2.8
OA	37 (15 M/22 F)	70.5 ± 10.4	72.1 ± 8.7	68.3 ± 8.7	12.9 ± 9.0	16.9 ± 2.8

(b)

Metric	Mean for older adults (OC)
MMSE	28.1 ± 1.7
ANART	12.9 ± 9.0
HVLT (immediate)	26.0 ± 6.8
TRAILS-A [s]	45.5 ± 19.9
TRAILS-B [s]	71.7 ± 24.1
GDS	4.0 ± 3.9
Systolic pressure	122.8 ± 16.1
Diastolic pressure	76.8 ± 10.1

MRI acquisition

All images were acquired using a Siemens Trio 3 Tesla system. The scans employed 12-channel phased-array head coil reception and body–coil transmission. A 3D anatomical was acquired using multi-echo MPRAGE (van der Kouwe et al., 2008), with resolution 1×1×1 mm, TR = 2530 ms, TI = 1000 ms, TE = 1.64, 3.50, 5.36 and 7.22 ms, field of view = 256×256 mm (sagittal), matrix size = 256×256×176, bandwidth = 651 Hz/voxel, and GRAPPA factor = 2.

Two pulsed ASL (PASL) datasets were obtained sequentially for each subject using the FAIR QUIPSS II PASL technique (Wang et al., 2002). A slice-selective frequency-offset corrected inversion (FOCI) pulse was applied during tag and control, the latter scan acquired in the absence of slab-selective gradients. The tag and control labelling thicknesses were 140 mm and 340 mm, respectively, leaving 100 mm margins at either end of the imaging slab to ensure optimal inversion profile. The QUIPSS II saturation pulse was applied to a 100 mm slab inferior to the imaging region with a 10 mm gap between the adjacent edges of the saturation and imaging slabs. Flow crusher gradients were applied with a threshold of 100 cm/s. Other imaging parameters were: 64×64 matrix, 24 slices (ascending interleaved acquisition), with a voxel size = 3.4×3.4×5 mm^3. The slice positioning and sample FAIR images area shown in Fig. 1. The PASL acquisitions each consisted of 104 frames (52 tag and 52 control), with TI1 = 600 ms and TI2 = 1600 ms, chosen to accommodate a wide range of flow rates. The scans used a repetition time (TR) of 4 s, and an echo-time (TE) of 12 ms, made possible by the current implementation of ¾ partial Fourier echo-planar imaging (EPI) readout, which enabled the minimization of BOLD effects and the reduction of susceptibility-related geometric distortions. The acquisition time per slice was 42 ms. A 2D gradient-echo EPI (echo-planar imaging) sequence was used in a calibration scan (with TR set to 10 s) to estimate the equilibrium magnetization of arterial blood. Sample images from the ASL acquisition are presented in Fig. 1.

Data processing

Structural assessments

All structural assessments were performed on the multi-echo MPRAGE images using the FreeSurfer image processing and analysis

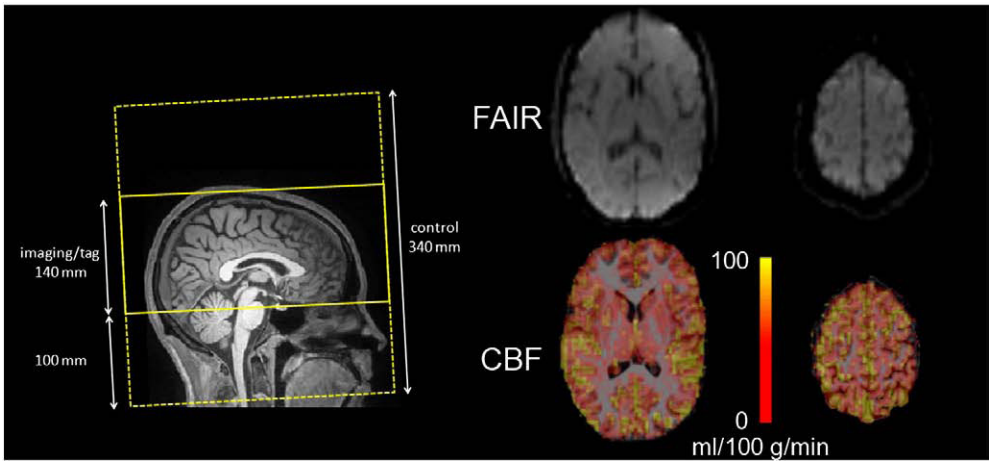

Fig. 1. The tagging and acquisition regions for the PASL scan are illustrated on the left. The PASL raw image and CBF maps (registered to the T_1-weighted anatomical images) are shown for an inferior (acquired earlier) and superior (acquire later) slice. The CBF maps demonstrate the expected PASL signal in cortical regions and subcortical grey matter, and low signal in white matter.

package (publically available at http://surfer.nmr.mgh.harvard.edu). The procedure includes removal of non-brain tissue using a hybrid watershed/surface deformation procedure (Segonne et al., 2004), automated transformation into the MNI152 standard space, intensity normalization (Sled et al., 1998), tessellation of the grey matter white matter boundary, automated topology correction (Segonne et al., 2007), and surface deformation following intensity gradients to optimally place the grey/white and grey/CSF borders at the location where the greatest shift in intensity defines the transition to the other tissue class (Fischl and Dale, 2000). The subsequent segmentation of the cortex and subcortical grey matter volumetric structures were performed for each subject based on probabilistic models of tissue magnetic resonance parameters and of anatomical locations (Fischl et al., 2004a,b). The resultant cortical models permitted surface inflation (Fischl et al., 1999a) and registration to a spherical atlas, whereby individual cortical folding patterns were used to match cortical geometry across subjects (Fischl et al., 1999b). Spherical registration has demonstrated superior accuracy than volume-based registration in aligning histological properties (Fischl et al., 2008).

Representations of cortical thickness, calculated as the closest distance from the grey/white boundary to the grey/CSF (cerebrospinal fluid) boundary at each vertex on the tessellated surface (Fischl and Dale, 2000), were produced using segmentation and deformation procedures based on both intensity and continuity information from the entire three dimensional MR volume. The resultant maps are sensitive to sub-millimeter differences in thickness between groups, and have been validated against histological analysis (Rosas et al., 2002) and manual measurements (Salat et al., 2004).

Quantitative CBF computation

The raw PASL time-series were motion- and drift-corrected using FLIRT (publically available at http://fsl.fmrib.ox.ac.uk/fsl/flirt), and subsequently divided into 52 tag-control pairs per acquisition. To minimize BOLD-contamination, the tag-control difference images were calculated using surround subtraction (Lu et al., 2006). Longitudinal (T_1) relaxation during the slice-dependent transit delays was compensated based on the per-slice acquisition time. The PASL volumes were then averaged across time and across the two datasets to maximize signal-to-noise, following which quantitative CBF maps were obtained according to the single-compartment Standard Kinetic Model (Buxton et al., 1998). The equilibrium arterial-blood magnetization was computed as the intensity in the calibration scan adjusted for longitudinal (T_1) and transverse relaxation (T_2^*) differences as well as blood–tissue water partition coefficient (λ). Typical values for proton density, λ, T_1 and T_2^* were assumed for all grey matter based on prior literature, as described in Çavuşoğlu et al. (2009). The labeling efficiency was assumed to be 98% (Wong et al., 1998a,b).

Group analysis

To enable surface and ROI-based analyses, the PASL data were upsampled to 1 mm^3 spatial resolution and registered to the native-space anatomical images using boundary-based registration (Greve and Fischl, 2009). Specifically, the mid-frame of the motion- and drift-corrected PASL time-series was chosen as the template image, and cross-modality registration was achieved by minimizing the misalignment between the cortical grey-white boundaries in the anatomical and PASL template images through 12 degree affine transforms. This method is minimally sensitive to differences in contrast and intensity non-uniformity in the two datasets, and the procedure benefited from the reduced geometric distortions in the PASL images through the short-TE partial-Fourier acquisition.

All segmentation-based volume ROIs were eroded by 1 mm around the perimeter to further reduce partial-volume contamination. Mean CBF values across volume ROIs were computed in native space, and regressed against age, both with and without using structural volume as a covariate. Cortical CBF reductions with age were assessed across the cortex and separately in the hippocampus. In addition, resting CBF in all cortical parcellations (Fischl et al., 2004b) was compared across hemispheres, genders and age-groups using multi-variate ANOVA.

To facilitate group-analysis, the anatomical-registered PASL data were sampled onto a surface atlas using spherical registration. The surface-sampling of the upsampled CBF maps was performed at a depth of 50% into the cortical ribbon. This approach was favoured over the inclusion of the entire cortex, despite the large voxel size in the source CBF images, as it was found to reduce the inclusion of voxels contaminated with white-matter or CSF. It was further cross-validated using the ROI-based approach described below. Group-mean CBF maps were generated using non-rigid high-dimensional spherical averaging (Fischl et al., 1999a). The interaction between cortical CBF and age was assessed by regressing out concurrent variations in cortical thickness, out of consideration for atrophy-related partial-volume contamination of CBF measures. Outliers were removed based on the standardized residuals (exclusion criterion = 2 standard deviations) prior to the regression analyses. General linear model-based statistical tests were performed with smoothing along the cortical surface using a circularly symmetric Gaussian kernel with a full-width at half-maximum (FWHM) of 10 mm, and the results were corrected for multiple comparisons using the false-discovery rate method (Genovese et al., 2002).

To visualize the interplay between resting CBF and thickness in aging-related changes, spatial overlaps were generated from regions showing

higher-than-average cortical CBF and/or thickness, and from those showing significant CBF reduction and/or cortical thinning. In addition, regions exhibiting the most significant age-associated CBF reduction were demarcated and analyzed individually, after regressing out variations in cortical thickness. To assess laterality effects (see Supplementary Materials), these regions were labelled ipsilaterally and matched to regions on the contralateral side. For this purpose, the surface labels were converted back into volume space through an extension into the cortical ribbon a depth of 10% to 90%. Furthermore, the thalamus, amygdala and accumbens, as well as substructures of the basal ganglia, were individually segmented, and their respective mean CBF values extracted for both hemispheres. Inter-hemispheric comparisons of CBF and grey-matter volume were also performed for all cortical and subcortical structures. All structural volume measures were corrected for estimated total intracranial volume (eTIV) using the atlas-scaling and covariance approach (Buckner et al., 2004). The significance of the regressions was computed using *t*-tests, and that of the inter-group comparisons were all performed using multi-factorial analysis of variance (ANOVA), with gender and/or age being the potential covariates.

Reproducibility analysis

Within-session cross-run reproducibility of the quantitative CBF measurements was assessed using the two PASL acquisitions acquired per subject, and quantified through the percent difference, that is, the absolute difference between the CBF values obtained from the two runs normalized by the cross-run CBF mean. In addition, to assess the reliability of the spatial localization of the cortical-thickness and CBF variations with age, we separated the full dataset (from all subjects) into two independent subsets of matched mean ages and sex ratios. One of these was used for the statistical analysis, based on the results of which regions of interest (ROIs) were delineated, and then mapped to the other subset. This methodology permitted us to assess and minimize cohort-specific effects in the observed CBF–age relationship.

Results

Effect of age on global CBF

The mean CBF value across the entire cortical grey matter volume was 52.6 ± 9.3, 52.0 ± 10.7, and 42.7 ± 8.8 ml/100 g/min in the young (YA), middle-aged (MA) and older (OA) adult groups, respectively. No significant difference was found between the YA and MA, but these latter were both found to differ from the OA group. The mean subcortical CBF, taken across the amygdala, accumbens, caudate, globus pallidus, putamen and thalamus, was 40.5 ± 7.6, 41.7 ± 7.1, and 39.5 ± 6.2 ml/100 g/min, respectively. One-tailed *t*-test revealed cortical CBF to exceed subcortical CBF in the YA ($p<0.001$), MA ($p<0.01$) but not the OA ($p=0.15$). Also, while there were no differences in mean CBF across hemispheres cortically ($p=0.90$) and subcortically ($p=0.91$), laterality effects were observed when examining select cortical ROIs (Table 2).

Spatial heterogeneities in CBF were also present, as seen in Fig. 2. The mean quantitative CBF values were mapped onto semi-inflated lateral (top) and medial (bottom) surface models in the YA, MA, and OA groups, as shown in Figs. 2a–c. The spatial variation in CBF was similar across age-groups, with OA exhibiting visibly reduced mean CBF compared both YA and MA, and the latter two showing a less remarkable mutual difference. There was also a spatially distinct pattern of variance in the CBF measurements (Fig. 2e). Lastly, we also illustrate the relationship between regional cortical thickness and colocalized CBF across individuals (Fig. 2f).

We evaluated the association between global CBF, tissue volume and age. Averaging across the entire cortex (encompassing both regions affected and unaffected by age), CBF was found to decrease at 0.38% per year ($p=0.014$) (Fig. 3a), amounting up to 27% over a 70-year period of adult life. In contrast, the slope for cortical volume vs. age (Fig. 3b) was 0.85% per year ($p=5.5\times10^{-8}$). Regression across all subcortical grey-matter structures as a whole revealed minimal decrease with age (Fig. 3c), although extensive negative correlations between tissue volume and age were observed across all subcortical structures studied (Fig. 3d). No significant pair-wise differences in global mean CBF were found among the age-groups, as shown by the group-average plots in Fig. 4. Cortical CBF was higher in women in the OA group ($p<0.05$) but not in the YA or MA groups. Although no statistically significant gender-disparity was found when all ages were pooled, subsequent statistical analyses examined effects controlled for sex.

Finally, lateralization and sex differences in CBF are presented in Table 2. In general, resting CBF was higher in the right hemisphere and in women (see Supplementary Materials).

Regional effects of age on CBF

Regional CBF values averaged across distinct cortical parcellations for the three age groups are shown in Table 2. The caudal middle-frontal, isthmus/posterior cingulate and pericalcarine regions were associated with higher CBF than the cortical average in all groups, although the differences were not statistically significant. ANOVA indicated a myriad of cortical parcellations displaying reductions in CBF in the OA as compared to the MA. In contrast, fewer regions exhibited such effects in the MA compared to the YA. Similar group trends pertain to the subcortical structures (Table 2), with Fig. 5 showing gender-dependence in individual parcellations. In the regression against age (Table 3), only the pallidum demonstrated a statistically significant effect.

We also evaluated the amplitude and statistical significance of CBF variations with age, shown in Figs. 6a, b, respectively. Interestingly, little spatial overlap is observed between the highest levels of CBF reduction and cortical thinning with age. This is further bolstered by the statistical results (Fig. 6c). Controlling for cortical thickness variations on a per-vertex basis did not have a substantial impact on the association between age and CBF, as demonstrated in Figs. 6c and d.

Reproducibility

The repeated PASL acquisition also facilitated the examination of cross-run CBF measurement repeatability in the same scan session. We found a mean CBF estimation difference of ≅7% (of group-mean) between scans, with no significant variation across cortical and subcortical structures. Furthermore, to determine the reliability of the observed regional CBF decreases, we divided the dataset into two samples, matched for both age and sex, with the first sample used to identify ROIs exhibiting significant age-associated CBF reduction (see Materials and methods). The ROIs were subsequently used to test for similar effects in the second sample, as described in our prior work (Salat et al., 2004; Salat et al., 2009). Significant regional CBF decline with age was robustly observed across these independent samples (see Supplementary Materials), as were the patterns of age-associated cortical thinning.

CBF and cortical thickness interactions

Cortical thinning was found to be largely bilateral, though stronger in the right hemisphere. Qualitative examination of potential mechanisms via various interactions between CBF and cortical thickness is presented in Fig. 7, including,

1. The overlap of regions showing age-associated decline in cortical thickness and in CBF (Fig. 7a) was used to address whether cortical thinning result from changes in CBF or vice versa), and we found that cortical thinning did not substantially overlap with regions showing the most notable CBF reductions;
2. The overlap between regions showing age-effects in CBF and high regional CBF in the young controls (Fig. 7b) was used to assess whether CBF decline later in life is driven by spatial bias early in life, and we

Table 2
Group-mean resting CBF values in all cortical parcellations and subcortical structures by cortical hemisphere, cortical hemisphere, and by age-group. (Note: $^{*}p<0.05$, $^{**}p<0.001$).

Strucuture		Mean CBF [ml/100 g/min]			Differences				
		YA	MA	OA	Left vs. right	Men vs. women	MA vs. YA	OA vs. YA	OA vs. MA
Cortical	Caudal anterior-cingulate	45.9 ± 8.8	43.3 ± 10.8	37.0 ± 7.9	L<R*	M<W*			
	Caudal middle-frontal	62.8 ± 12.4	56.1 ± 15.7	49.8 ± 15.7	L<R*	M<W*		OA<YA*	OA<MA*
	Cuneus	53.2 ± 6.7	52.2 ± 20.5	39.4 ± 16.5					
	Entorhinal	40.4 ± 17.9	41.9 ± 18.3	33.3 ± 7.9	L<R*	M>W*			
	Fusiform	46.1 ± 9.3	46.6 ± 13.0	39.5 ± 8.4	L>R*				
	Hippocampus	45.7 ± 8.0	48.7 ± 10.0	43.7 ± 8.6	L<R*				
	Inferior parietal	56.7 ± 9.8	55.2 ± 11.9	44.6 ± 11.9	L>R**	M<W**	MA<YA*	OA<YA*	OA<MA**
	Inferior temporal	47.1 ± 8.8	43.8 ± 23.2	36.0 ± 14.9					
	Insula	47.7 ± 8.2	47.3 ± 9.4	37.3 ± 8.1	L<R**	M<W*			OA<MA*
	Isthmus cingulate	58.8 ± 12.4	57.7 ± 16.1	45.4 ± 9.3	L<R**				
	Lateral occipital	55.2 ± 12.6	57.7 ± 19.9	46.0 ± 13.6	L>R**				
	Lateral orbitofrontal	46.1 ± 8.5	47.0 ± 10.3	39.8 ± 8.6	L>R**				
	Lingual	53.2 ± 11.4	56.1 ± 12.5	52.2 ± 10.5					
	Medial orbitofrontal	42.5 ± 7.9	41.6 ± 9.1	34.6 ± 8.4	L>R**				
	Middle temporal	53.6 ± 9.6	53.0 ± 11.2	44.6 ± 11.0	L<R**				
	Parahippocampal	42.5 ± 12.1	42.4 ± 12.2	36.2 ± 7.6	L<R*				
	Paracentral	52.1 ± 11.7	53.5 ± 10.2	49.5 ± 9.3		M<W*		OA<YA*	OA<MA*
	Parsopercularis	52.2 ± 9.2	49.5 ± 10.4	42.5 ± 9.4	L<R**	M<W*		OA<YA*	OA<MA*
	Parsorbitalis	47.8 ± 8.5	53.7 ± 34.5	40.9 ± 10.5	L>R*			OA<YA*	
	Parstriangularis	53.4 ± 9.7	50.8 ± 11.2	44.2 ± 9.3	L>R**	M<W*			OA<MA*
	Pericalcarine	58.4 ± 7.6	59.8 ± 12.1	52.7 ± 12.3	L>R*	M<W*			OA<MA*
	Postcentral	50.2 ± 10.4	48.9 ± 10.6	42.6 ± 9.2	L<R**	M<W*		OA<YA*	OA<MA*
	Posterior cingulate	59.9 ± 10.5	55.0 ± 12.0	45.1 ± 11.0	L<R**	M<W**		OA<YA*	OA<MA*
	Precentral	55.2 ± 10.4	54.5 ± 11.7	48.8 ± 9.6	L>R*	M<W*		OA<YA*	OA<MA*
	Precuneus	51.4 ± 8.7	50.0 ± 10.6	43.3 ± 11.5	L<R**	M<W*		OA<YA*	OA<MA*
	Rostral anterior cingulate	36.5 ± 5.4	35.4 ± 7.8	31.9 ± 6.7	L>R*				
	Rostral middle-frontal	49.3 ± 9.9	45.2 ± 11.3	38.1 ± 11.2	L>R**	M<W**	MA<YA*	OA<YA*	OA<MA*
	Superior frontal	57.1 ± 8.4	52.9 ± 11.0	46.5 ± 9.4	L>R**	M<W*		OA<YA*	OA<MA*
	Superior parietal	51.4 ± 12.1	46.3 ± 15.4	35.9 ± 12.4	L<R**	M<W*		OA<YA*	
	Superior temporal	47.1 ± 9.3	47.4 ± 9.0	42.5 ± 9.3	L<R*	M<W*		OA<YA*	
	Supramarginal	52.7 ± 11.2	49.3 ± 10.0	43.7 ± 7.7	L>R**	M<W**	MA<YA*	OA<YA*	OA<MA*
	Frontal pole	42.9 ± 9.7	41.0 ± 15.8	33.2 ± 14.2	L>R*	M<W*		OA<YA*	OA<MA*
	Temporal pole	40.8 ± 9.1	37.4 ± 13.3	35.3 ± 9.6					
	Transverse temporal	60.7 ± 12.5	64.3 ± 14.1	55.7 ± 15.1					
	Mean	**52.6 ± 9.3**	**52.0 ± 10.7**	**42.7 ± 8.8**					
Subcortical	Accumbens	37.1 ± 8.4	37.7 ± 7.4	37.1 ± 9.1					
	Amygdala	36.9 ± 10.6	39.5 ± 9.5	36.1 ± 8.9					
	Caudate	46.1 ± 7.7	44.9 ± 7.1	42.1 ± 8.4	L<R*	M<W**		OA<YA*	OA<MA*
	Pallidum	26.3 ± 6.1	28.4 ± 5.1	28.0 ± 6.7		M<W*		OA<YA*	OA<MA*
	Putamen	46.8 ± 8.2	45.7 ± 7.7	44.7 ± 8.4		M<W*			
	Thalamus	44.8 ± 5.2	47.0 ± 10.4	45.1 ± 9.4				OA<YA*	
	Mean	**40.5 ± 7.6**	**41.7 ± 7.1**	**39.5 ± 6.2**					

found this link to be limited to the temporal, parietal and precuneus regions;

3. The overlap between regions of high CBF in young adults and those showing associations between cortical thickness and age (Fig. 7c) was used to assess whether high resting CBF was related to predisposition for cortical thinning, and substantial overlap was observed;
4. The coexistence of age-associations in CBF and high cortical thickness in young adults (Fig. 7d) was used to assess if changes in CBF occur selectively in thicker or thinner regions of cortex, and we found regions of reduced CBF not to be directly associated with thickness.

Discussion

This study investigated the relationship between cerebral perfusion and aging. Reproducibility associated with pulsed ASL CBF measurements is in agreement with previous findings (Jiang et al., 2010; Parkes et al., 2004). We demonstrated substantial spatial non-uniformity in CBF cortically and subcortically, independent of age. Significant age-associated regional CBF reduction was widely observed throughout the cortex. Importantly, these reductions were not closely associated with age-related cortical thinning. In contrast, a suggestive relationship was found between CBF in young adults and cortical thinning in aging. This potential link to mechanisms of age-associated atrophy is of interest for future examination. Given previous evidence of an important relationship between pathological perfusion reduction and neuronal degeneration (Fierstra et al., 2010), the current findings may indicate a distinct paradigm characteristic of normal aging. Lastly, the spatial distribution of CBF reductions spans regions reported to be involved in default-mode activity (for review see Raichle and Snyder, 2007), warranting further investigation.

CBF reduction in aging

Our CBF estimates are consistent with values in the PET and MRI literature (Calamante et al., 1999; Çavuşoğlu et al., 2009; Leenders et al., 1990; Shin et al., 2007), and particularly with prior findings using ASL (Wong et al., 1998b; Ye et al., 1997; Zou et al., 2009). The loci of low and high perfusion are in agreement with numerous reports using PET (Ishii et al., 1996; Leenders et al., 1990; Raichle et al., 2001) and CASL (Lee et al., 2009; Zou et al., 2009).

The inter-group comparisons of mean CBF in parcellations revealed more regions with age-related CBF decrease than did the per-vertex surface-regression analyses. In fact, the use of the two approaches served as self check for consistency, and we found aging-associated cortical CBF reduction to be greatest later in life (after the transition from middle-aged to older-adults) instead of being a linear process. Nonetheless, our data is under-powered for demonstrating significant nonlinear trends, given the inter-subject variability.

Reproducible cross-sectional age-effects in CBF were demonstrated with negligible cohort differences between, the localization of which

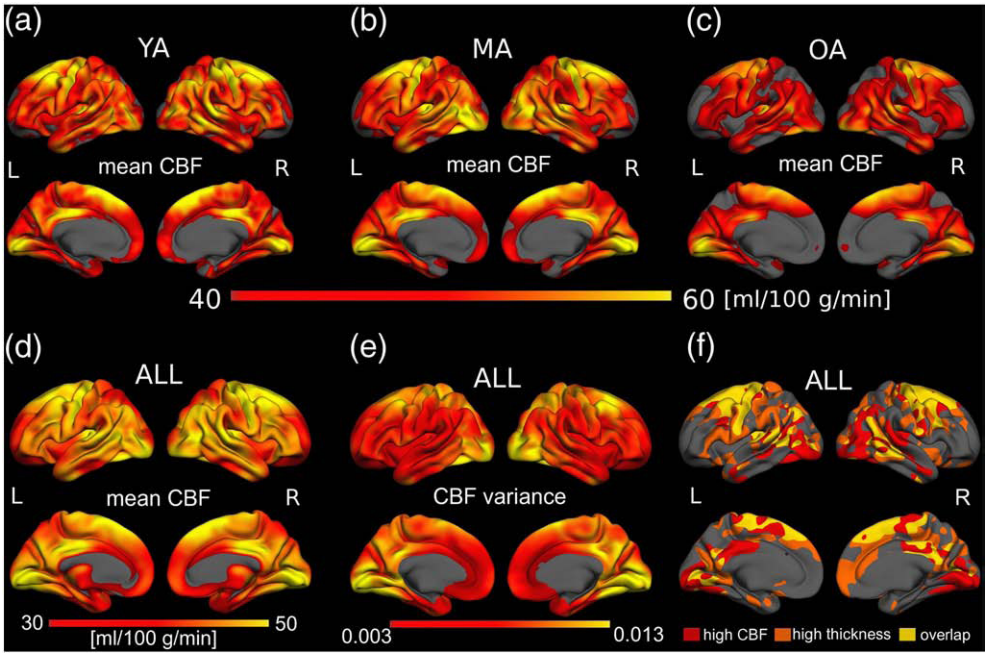

Fig. 2. Quantitative CBF values across the cortex. Average cortical quantitative CBF for the YA (a), MA (b) and OA (c) groups were mapped onto semi-inflated lateral (top) and medial (bottom) surface models. Across all groups, the highest resting CBF was found to be associated mainly with visual and motor areas, in addition to the superior frontal region and the posterior cingulate, confirmed in the average over all subjects (d). The variance in CBF across cortical regions is demonstrated in (e), and may affect the statistical power of age effects. Lastly, the spatial variation in CBF is similar across age-groups, with the older-adults showing visibly reduced CBF. Regions of high mean basal CBF did not directly translate to high cortical thickness (f).

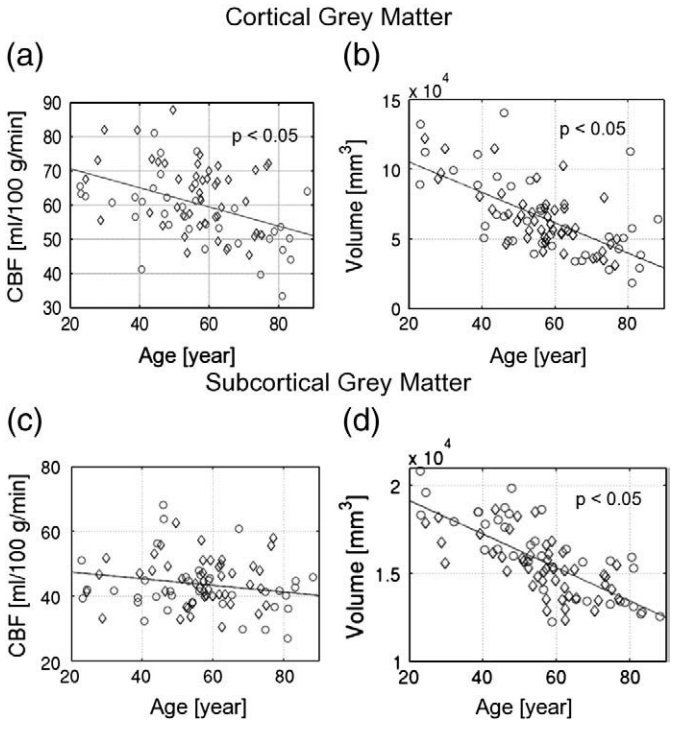

Fig. 3. Association between global cortical CBF, tissue volume and age. Men are indicated by circles and women by diamonds, and regression models are shown as solid lines. The mean CBF across the entire cortex was negatively correlated with age (a), with a slope of −0.38% per year ($p<0.05$). Cortical grey matter volume, normalized by total intracranial volume, also shows a negative association with age, with a slope of 0.85% per year ($p<0.05$), exceeding concurrent reductions in CBF. On the other hand, the CBF averaged across all subcortical structures did not significantly vary with age (c), while subcortical grey-matter volume variations were associated with a slope of −0.44% per year ($p<0.05$). All volume measures were corrected for intracranial volume (eTIV).

corresponding to a superset of regions implicated in aging in previous $H_2^{15}O$ PET and CASL studies, including the frontal and insular cortices (Leenders et al., 1990), the frontal–temporal region (Beason-Held et al., 2009; Inoue et al., 2005; Lee et al., 2009; Pagani et al., 2002), the precuneus (Beason-Held et al., 2009; Lee et al., 2009), and the anterior cingulate (Pagani et al., 2002). The left hemisphere was associated with a greater number of regions with reduced CBF than the right hemisphere, specifically the lateral occipital and supramarginal regions, in agreement with PET findings (Pagani et al., 2002), though there was little hemispheric bias in the rates of CBF reduction.

Our measurements of the CBF–age relationship in the frontal and insular regions are in excellent agreement with observations by Leenders et al., while those in the superior frontal region and precuneus are in agreement with longitudinal findings by Beason-Held et al. (2009). The CBF decline in the frontal, temporal, and parietal regions are macroscopically in agreement with CT findings both cross-sectionally and longitudinally (Akiyama et al., 1997), although Akiyama et al. noted an absence of longitudinal effects in the occipital lobe, in contrast to their cross-sectional results and to our own results. Also, our finding of

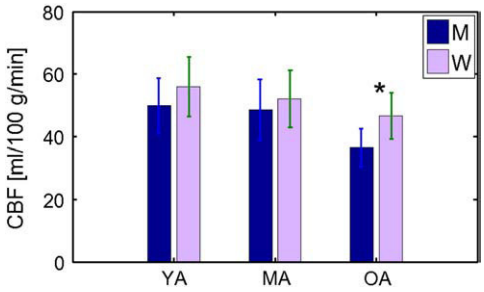

Fig. 4. Global average CBF values in the cortex. Cortical CBF in young (YA), middle aged (MA), and older adults (OA) differentiated by sex (men, M, and women, W). The average CBF across the entire cortex was higher in women in the OA group (denoted by asterisk), but there was no gender-dependence globally in the YA or MA groups. Also evident from this group comparison is a trend for OA to have reduced CBF compared to YA and MA, although the difference eluded statistical significant for either the men or the women.

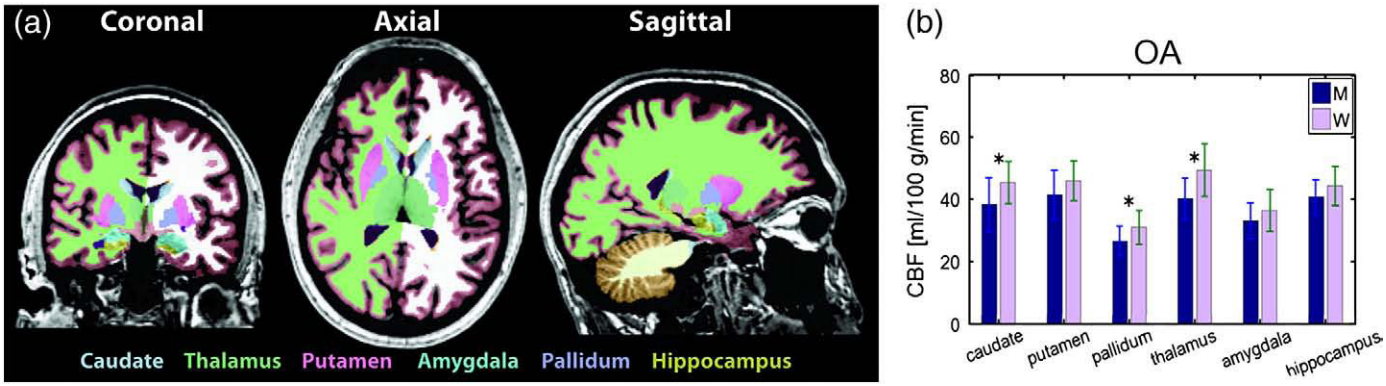

Fig. 5. Mean CBF values in subcortical grey-matter volumes and in the hippocampus, as labelled in (a), demonstrate a difference between men (M) and women (W) for the OA age-group only (b).

reduced CBF in the superior parietal region is in contrast with reports by Beason-Held et al. (2009), potentially as the latter was a longitudinal study focusing on an age-range truncated to involve only older adults (age = 68.4 ± 6.8 years). A key future goal will be to study the potential disparities between longitudinal and cross-sectional assessments.

In the subcortex, our observation of reduced perfusion in the caudate and thalamus in the OA is consistent with CT findings (Akiyama et al., 1997), although unlike Akiyama et al., we did not observe significant CBF–age relationship in the putamen. Finally, despite prior findings of augmented subcortical perfusion in healthy older adults (Lee et al., 2009; Pagani et al., 2002), such increases with age were not found in the present setting; such effects may be attributed to partial-volume contamination (Barnden et al., 2005). It should be noted, however, that prior SPECT studies examined CBF normalized by global flow, implying that an unchanged subcortical CBF may seem to be an increase, should global CBF be reduced.

In terms of mean cortical CBF, the sex-difference was only significant in the older adults, perhaps owing to the substantial inter-subject variability within groups. CBF disparities between genders spatially selective, with women consistently being associated with higher CBF, also in accordance with prior results (Jones et al., 1998; Li et al., 2004; Parkes et al., 2004; Shin et al., 2007). As to the slope of CBF vs. age, no significant gender bias was found, echoing previously findings in whole-brain analyses (Buijs et al., 1998), but contrary to select PET and MRI experiments (Pagani et al., 2002; Shin et al., 2007).

The currently observed whole-cortex CBF reduction of ~0.38% per year is lower than previously reported whole-brain (~0.52% per year, using 2D phase-contrast cerebral angiography) (Buijs et al., 1998) and whole-cortical measurements (0.76% per year, using contrast-enhanced MRI) (Shin et al., 2007), but more comparable with CASL-based findings (Parkes et al., 2004). Several factors may contribute to the differences, including the inclusion of white matter in the estimation of whole-head perfusion and the subject selection criteria (such as the inclusion of individuals with cognitive deficits and/or macrovascular pathology). In addition, previous studies have been more limited in slope, owing in part to the invasive nature of traditional perfusion imaging techniques — the non-invasiveness and high accessibility of pulsed ASL imaging was integral to achieving comprehensiveness in our cohort. Moreover, earlier perfusion quantification techniques were sensitive to limitations in temporal (Chen et al., 2005a; Østergaard et al., 1996) and spatial resolution (Chen et al., 2005b; Inoue et al., 2005; Inoue et al., 2003; Law et al., 2000; Meltzer et al., 2000). From the latter perspective, the effect of atrophy is of particular importance to aging studies, and the interpretation of CBF changes is ideally made in conjunction with structural changes.

Knowledge of the patterns of age-associated CBF decline is invaluable for distinguishing normal changes from more detrimental disease-related degeneration. While much of our findings resemble SPECT-based observations in dementia (Matsuda et al., 2002, 2003) and more recently using CASL (Dai et al., 2009; Hayasaka et al., 2006; Nagata et al., 2000; Schuff et al., 2009; Shimizu et al., 2010; Yang et al., 2002) and AD (Tosun et al., 2010), some exceptions were found, such as in the amygdala (Dai et al., 2009) and hippocampus (Alsop et al., 2008; Dai et al., 2009; Fleisher et al., 2009; Heo et al., 2010; Ito et al., 2006; Nagata et al., 2000).

Association between CBF reductions and tissue atrophy

The spatial distribution of cortical thinning with age in the current cohort was robustly observed across independent samples, and in agreement with previous reports based on both MRI (Fjell et al., 2009; Raz et al., 1997; Salat et al., 2004) and CT (Akiyama et al., 1997). These results correspond well with those identified by the latter work as exhibiting the most robust cortical thinning. Further agreement was found with other previous MRI-based findings (Burgmans et al., 2009; Raz et al., 2003; Sullivan et al., 2004; Walhovd et al., 2005), although the shrinkage was less pronounced than previously reported.

Based on prior knowledge linking perfusion deficit and tissue damage (Fierstra et al., 2010; Koehler et al., 2009), we hypothesized that CBF reduction and tissue atrophy would be closely related in aging. However, a key finding of this work is to the contrary. Specifically, although regions which exhibit significant cortical thinning, such as the frontal, temporal and precuneus regions, also exhibit reduced perfusion, in agreement with findings by Tosun et al. (2010), there were many regions showing reduced cortical thickness without a concomitant reduction in CBF. Furthermore, the association between CBF and age was minimally influenced by neutralizing the effect of cortical thinning. This relative dissociation of CBF reduction and atrophy in aging builds upon potentially related observations in healthy older adults examined with PET by Sojkova et al. (2010) but are not consistent with earlier CT results in aging (Akiyama et al., 1997; Obara et al., 1994). The times of occurrence of CBF and tissue volume reductions are likely to differ, the significance thereof remaining to be clarified.

Stemming from neurovascular coupling requirements, the influence of age on CBF is likely to reflect underlying changes in neuronal activity.

Table 3
Regression of CBF against age (controlling for grey-matter volume as covariate) and cortical thickness in key grey-matter volumes. Bold figures indicate statistically significant changes.

Structure	Slope of CBF vs. age [%/year]	p	Slope volume vs. age [%/year]	p
Accumbens	0.23	0.54	**−0.75**	1.4×10^{-6}
Amygdala	−0.10	0.85	**−0.44**	9.2×10^{-8}
Caudate	−0.18	0.13	**−0.35**	0.0041
Pallidum	**−0.05**	0.02	**−0.53**	4.4×10^{-5}
Putamen	−0.06	0.86	**−0.54**	4.4×10^{-10}
Thalamus	−0.11	0.78	**−0.43**	1.0×10^{-11}
Subcortex	−0.09	0.76	**−0.44**	2.7×10^{-14}
Hippocampus	0.04	0.05	**−0.50**	3.1×10^{-10}
Cortex	**−0.38**	0.001	**−0.83**	8.2×10^{-10}

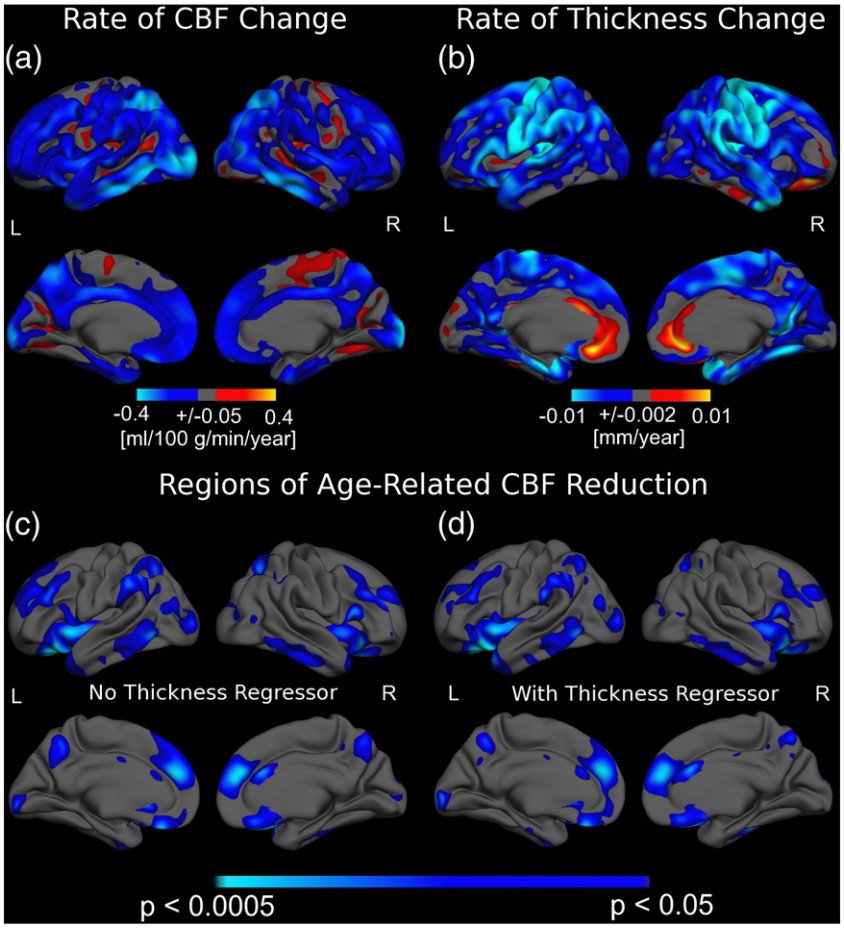

Fig. 6. The association between age and regional CBF as well as cortical thickness. The colour scales in (a) and (b) indicate the amplitude of age-associations in CBF, while that in (c) and (d) indicates statistical significance, with light blue and yellow denoting the strongest negative and positive associations, respectively. Regions exhibiting the largest magnitude of CBF reduction (a) and cortical thinning with age (b) did not spatially coincide. The significance map of CBF reductions before (c) and after vertex-wise covariation for age-associations in cortical-thickness (d) only subtly differed. Greatest statistical effects were found in the left supramarginal and occipital gyri, and the right anterior cingulate, as well as bilaterally in the right rostral middle-frontal, superior parietal, middle-inferior temporal and insular regions, medial superior frontal, orbito-frontal and precuneus regions. Furthermore, the localization of regions exhibiting the most rapid age-related CBF decline appeared to coincide with regions showing the highest statistical effects of age on CBF.

Age-related and comparable decreases in CBF and $CMRO_2$ have been reported previously (Leenders et al., 1990; Pantano et al., 1984), particularly in the parietal (Burns and Tyrrell, 1992), frontal and temporal lobes (Burns and Tyrrell, 1992; Leenders et al., 1990), coinciding with locations showing CBF reduction in this study. It is unclear whether basal flow and/or metabolism are related to resistance to cerebrovascular degeneration in aging/dementia. Our results qualitatively demonstrate a parallel between reduced CBF and elevated resting oxidative metabolism (Buckner et al., 2005; Gjedde et al., 2005; Raichle et al., 2001), a set of regions widely referred to as part of the default-mode network. The significance of this finding will be further investigated. Finally, the development of hyper- or hypotension, particular in the MA and OA populations, has been suggested as a contributor to CBF changes (Alves and Busatto, 2006; Gruhn et al., 2001).

While the relationship between concurrently observed CBF reduction and cortical atrophy has previously been investigated using a voxel-based morphometric (VBM) approach, existing VBM results have not been consistent (Ito et al., 2006; Van Laere and Dierckx, 2001), perhaps due to such limiting factors as spatial resolution and common uncertainties in the accuracy of volume-based registration for atlas-based analyses (Greve and Fischl, 2009; Zollei et al., 2010), particularly in view of complications introduced by age-related atrophy (Dai et al., 2008a). Our findings build upon prior work by Tosun et al. (2010), in which surface mapping was used to demonstrate dissociations between CBF and cortical thickness reductions in individuals with AD. We did not compensate the CBF values themselves for intra-voxel tissue heterogeneity (Asllani et al., 2008), but instead regressed out the contribution of grey-matter volume variations from the association between CBF and age. Finally, our results are based on the largest perfusion and structural MRI datasets acquired to-date for such investigations on aging, and the outcome of our surface-based group-analyses was further confirmed by the results of our subject-specific native-space volume-based ROI-analyses.

Limitations and caveats

Pulsed ASL is known for its sensitivity to arterial-transit delay, which may be lengthened in aging. In addition, in the healthy subjects, the inferior half of the brain is reportedly associated with longer transit delays (Qiu et al., 2010), while relatively long delays have also been associated the frontal and occipital lobes (MacIntosh et al., 2010). As these factors are important determinants of CBF accuracy, our PASL parameters were chosen to minimize velocity-related bias. Specifically, a relatively short TI_1 of 600 ms facilitated the minimization of bolus-width sensitivity even for rapid flow, common to younger subjects, while a TI_2 of 1600 ms exceeds the longest grey-matter transit delay (cortical and subcortical) expected in healthy adults (Qiu et al., 2010), accommodating the slower flow which may be expected in certain older adults. Furthermore, the cortical and subcortical CBF reduction patterns in aging observed in this study differ spatially from the patterns of transit delay heterogeneity. Thus, it is not likely that the observed changes are driven primarily by the above PASL-

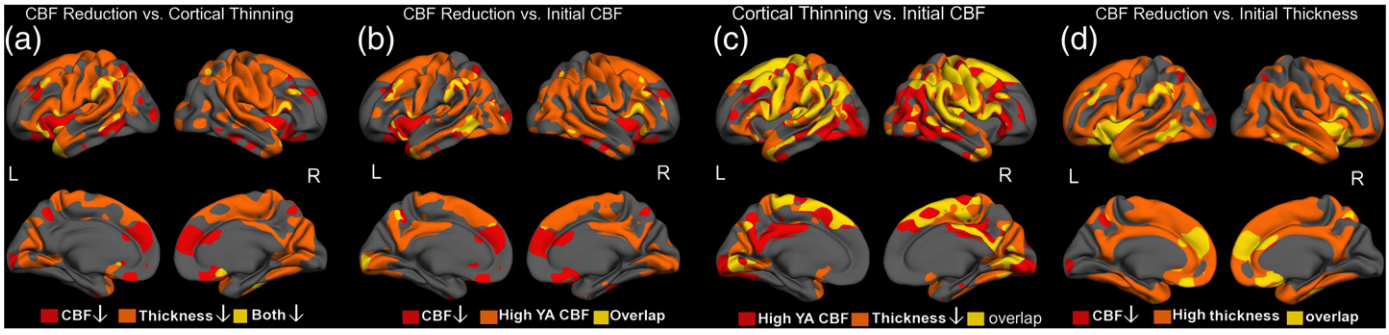

Fig. 7. Associations between resting CBF, cortical thickness and their respective magnitudes of age-association. Regions of high thickness and CBF were defined as those with values exceeding the cortical mean. There was minimal overlap between regions showing age-associated cortical thinning and regions showing age-related decrease in CBF (a). Regions showing the highest CBF in youth (represented by mean CBF in YA group) were not necessarily those showing the greatest cross-sectional age-associated CBF reductions (b). Interestingly, there was substantially more overlap between regions of high CBF and greatest thickness reductions, although the overlap did not encompass all regions manifesting cortical thinning (c). Finally, almost all regions of high cortical thickness are associated with significant CBF reduction, the latter having been controlled for concurrent thickness decrease (d).

related artifacts and biases, although it is possible that arterial transit times may contribute in some way to the reported effects. Additionally, ASL measures of CBF are dependent on tissue and blood T_1 and T_2^*. These parameters have been found to decrease with advancing age in brain tissue (Cho et al., 1997; Mitsumori et al., 2009). Based on these prior findings, we estimated the worst-case errors using numerical simulations (data not shown), and found these figures to translate to a CBF underesmation of up to ~10% (T_2-related) and CBF overestimation of up to ~8% (T_1-related), respectively. Notwithstanding, these opposite and competing effects are exceeded by the CBF reductions currently reported. Nonetheless, prospectively, we hope to study the effect of physiological changes in aging on CBF measurement (Wu et al., 2009), and to enhance the sensitivity of our CBF measures using novel pseudo-continuous ASL techniques (Xu et al., 2010).

Importantly, the current study presents a cross-sectional view on aging. We are aware of the potential confounds of cross-sectional studies, such as cohort effects. To assess the potential influence of cohort effects, we have repeated the analyses on two independent sample populations, and arrive at similar results. Furthermore, our results are compatible with previous longitudinal findings (Sojkova et al., 2008), although we noted slight discrepancies partially due to differences in the subjects' age range. More detailed examinations of the comparability of cross-sectional to longitudinal findings will be one of the key targets for future efforts.

Conclusions

An accurate understanding of cerebral perfusion changes in normal aging is key to deciphering the neurovascular manifestations and pathogenesis of age-related neurological diseases. This work is the first instance in which surface processing procedures are used to map in detail MR measures of perfusion and structural changes associated with normal aging. We have demonstrated regionally specific grey matter perfusion variations across the adult lifespan using pulsed ASL. Our results demonstrate that regions of CBF reduction are largely distinct from those most burdened by grey-matter atrophy, suggesting differential contributions to age-related cognitive decline by hemodynamic and structural changes. Furthermore, the age-associated CBF decreases were most significant in regions commonly associated with higher resting metabolism. This work sets the stage for a larger scale use of pulsed ASL to investigate perfusion alterations in cerebrovascular disease and dementia.

Supplementary materials related to this article can be found online at doi:10.1016/j.neuroimage.2010.12.032.

Acknowledgments

This research was supported by NIH grants K01AG024898, R01NR010827, NS042861, and P41RR14075, as well as the Canadian Institutes of Health Research (CIHR) and the Athinoula A. Martinos Center for Biomedical Imaging. We also thank Dr. Doug Greve for his input on multi-modal image registration, and Mr. Robert McInnis for help with cognitive testing.

References

Aguero-Torres, H., Kivipelto, M., von Strauss, E., 2006. Rethinking the dementia diagnoses in a population-based study: what is Alzheimer's disease and what is vascular dementia? A study from the Kungsholmen project. Dementia and Geriatric Cognitive Disorders 22, 244–249.

Akiyama, H., Meyer, J.S., Mortel, K.F., Terayama, Y., Thornby, J.I., Shizuko, K., 1997. Normal human aging: factors contributing to cerebral atrophy. Journal of the Neurological Sciences 152, 39–49.

Alsop, D.C., Casement, M., de Bazelaire, C., Fong, T., Press, D.Z., 2008. Hippocampal hyperperfusion in Alzheimer's disease. Neuroimage 42, 1267–1274.

Alsop, D.C., Dai, W., Grossman, M., Detre, J.A., 2010. Arterial spin labeling blood flow MRI: its role in the early characterization of Alzheimer's disease. Journal of Alzheimer's Disease 20, 871–880.

Alves, T.C., Busatto, G.F., 2006. Regional cerebral blood flow reductions, heart failure and Alzheimer's disease. Neurological Research 28, 579–587.

Asllani, I., Borogovac, A., Brown, T.R., 2008. Regression algorithm correcting for partial volume effects in arterial spin labeling MRI. Magnetic Resonance in Medicine 60, 1362–1371.

Barnden, L.R., Behin-Ain, S., Kwiatek, R., Casse, R., Yelland, L., 2005. Age related preservation and loss in optimized brain SPECT. Nuclear Medicine Communications 26, 497–503.

Beason-Held, L.L., Kraut, M.A., Resnick, S.M., 2009. Stability of default-mode network activity in the aging brain. Brain Imaging Behav 3, 123–131.

Bell, R.D., Zlokovic, B.V., 2009. Neurovascular mechanisms and blood-brain barrier disorder in Alzheimer's disease. Acta Neuropathologica 118, 103–113.

Breteler, M.M., 2000. Vascular risk factors for Alzheimer's disease: an epidemiologic perspective. Neurobiology of Aging 21, 153–160.

Buckner, R.L., Head, D., Parker, J., Fotenos, A.F., Marcus, D., Morris, J.C., Snyder, A.Z., 2004. A unified approach for morphometric and functional data analysis in young, old and demented adults using automated atlas-based head size normalization: reliability and validation against manual measurement of total intracranial volume. Neuroimage 23, 724–738.

Buckner, R.L., Snyder, A., Shannon, B.J., LaRossa, G., Sachs, R., Fotenos, A.F., Sheline, Y.I., Klunk, W.E., Mathis, C.A., Morris, J.C., Mintun, M.A., 2005. Molecular, structural, and functional characterizatioin of Alzheimer's disease: evidence for a relationship between default activity, amyloid, and memory. Neurobiology of Aging 25, 7709–7717.

Buijs, P.C., Krabbe-Hartkamp, M.J., Bakker, C.J., de Lange, E.E., Ramos, L.M., Breteler, M.M., Mali, W.P., 1998. Effect of age on cerebral blood flow: measurement with ungated two-dimensional phase-contrast MR angiography in 250 adults. Radiology 209, 667–674.

Burgmans, S., van Boxtel, M.P., van den Berg, K.E., Gronenschild, E.H., Jacobs, H.I., Jolles, J., Uylings, H.B., 2009. The posterior parahippocampal gyrus is preferentially affected in age-related memory decline. Neurobiology of Aging (Electronic publication ahead of print). doi:10.1016/j.neurobiolaging.2009.09.008.

Burns, A., Tyrrell, P., 1992. Association of age with regional cerebral oxygen utilization: a positron emission tomography study. Brain 21, 316–320.

Buxton, R.B., Frank, L.R., Wong, E.C., Siewert, B., Warach, S., Edelman, R.R., 1998. A general kinetic model for quantitative perfusion imaging with arterial spin labeling. Magnetic Resonance in Medicine 40, 383–396.

Calamante, F., Thomas, D.L., Pell, G.S., Wiersma, J., Turner, R., 1999. Measuring cerebral blood flow using magnetic resonance imaging techniques. Journal of Cerebral Blood Flow and Metabolism 19, 701–735.

Caroli, A., Testa, C., Geroldi, C., Nobili, F., Barnden, L.R., Guerra, U.P., Bonetti, M., Frisoni, G.B., 2007. Cerebral perfusion correlates of conversion to Alzheimer's disease in amnestic mild cognitive impairment. Journal of Neurology 254, 1698–1707.

Çavuşoğlu, M., Pfeuffer, J., Uğurbil, K., Uludağ, K., 2009. Comparison of pulsed arterial spin labeling encoding schemes and absolute perfusion quantification. Magnetic Resonance Imaging 27, 1039–1045.
Chen, J.J., Smith, M.R., Frayne, R., 2005a. The advantages of frequency domain modeling in DSC MR CBF quantification. Magnetic Resonance in Medicine 53, 700–707.
Chen, J.J., Smith, M.R., Frayne, R., 2005b. Partial-volume effects in DSC MR perfusion quantification. Journal of Magnetic Resonance Imaging 22, 390–399.
Cho, S., Jones, D.K., Reddick, W.E., Ogg, R.J., Steen, R.G., 1997. Establishing norms for age-related changes in proton T1 of human brain tissue in vivo. Magnetic Resonance Imaging 15, 1133–1143.
Dai, W., Carmichael, O.T., Lopez, O.L., Becker, J.T., Kuller, L.H., Gach, H.M., 2008a. Effects of image normalization on the statistical analysis of perfusion MRI in elderly adults. Journal of Magnetic Resonance Imaging 28, 1351–1360.
Dai, W., Garcia, D., De Bazelaire, C., Alsop, D.C., 2008b. Continuous flow-driven inversion for arterial spin labeling using pulsed radio frequency and gradient fields. Magnetic Resonance in Medicine 60, 1488–1497.
Dai, W., Lopez, O.L., Carmichael, O.T., Becker, J.T., Kuller, L.H., Gach, H.M., 2008c. Abnormal regional cerebral blood flow in cognitively normal elderly subjects with hypertension. Stroke 39, 349–354.
Dai, W., Lopez, O.L., Carmichael, O.T., Becker, J.T., Kuller, L.H., Gach, H.M., 2009. Mild cognitive impairment and alzheimer disease: patterns of altered cerebral blood flow at MR imaging. Radiology 250, 856–866.
de la Torre, J.C., 2005. Is Alzheimer's disease preceded by neurodegeneration or cerebral hypoperfusion? Annals of Neurology 57, 783–784.
Detre, J.A., Alsop, D.C., Samuels, O.B., Gonzalez-Atavales, J., Raps, E.C., 1998a. Cerebravascular Reserve Testing Using Perfusion MRI with Arterial Spin Labeling in Normal Subjects and Patients with Cerebrovascualr Disease. Proceedings of the ISMRM, Sydney.
Detre, J.A., Alsop, D.C., Vives, L.R., Maccotta, L., Teener, J.W., Raps, E.C., 1998b. Noninvasive MRI evaluation of cerebral blood flow in cerebrovascular disease. Neurology 50, 633–641.
Detre, J.A., Leigh, J.S., Williams, D.S., Koretsky, A.P., 1992. Perfusion imaging. Magnetic Resonance in Medicine 23, 37–45.
Detre, J.A., Zhang, W., Roberts, D.A., Silva, A.C., Williams, D.S., Grandis, D.J., Koretsky, A.P., Leigh, J.S., 1994. Tissue specific perfusion imaging using arterial spin labeling. NMR in Biomedicine 7, 75–82.
Dickstein, D.L., Walsh, J., Brautigam, H., Stockton Jr., S.D., Gandy, S., Hof, P.R., 2010. Role of vascular risk factors and vascular dysfunction in Alzheimer's disease. The Mount Sinai Journal of Medicine 77, 82–102.
Driscoll, I., Zhou, Y., An, Y., Sojkova, J., Davatzikos, C., Kraut, M.A., Ferrucci, L., Mathis, C.A., Klunk, W.E., Wong, D.F., Resnick, S.M., 2010. Lack of association between ^{11}C-PiB and longitudinal brain atrophy in non-demented older individuals. Neurobiology of Aging. doi:10.1016/j.neurobiolaging.2009.12.008.
Duron, E., Hanon, O., 2010. Antihypertensive treatments, cognitive decline, and dementia. Journal of Alzheimer's Disease 20, 903–914.
Elias, M.F., D'Agostino, R.B., Elias, P.K., Wolf, P.A., 1995. Neuropsychological test performance, cognitive functioning, blood pressure, and age: the Framingham Heart Study. Experimental Aging Research 21, 369–391.
Farmer, M.E., Kittner, S.J., Abbott, R.D., Wolz, M.M., Wolf, P.A., White, L.R., 1990. Longitudinally measured blood pressure, antihypertensive medication use, and cognitive performance: the Framingham Study. Journal of Clinical Epidemiology 43, 475–480.
Fierstra, J., Poublanc, J., Han, J.S., Silver, F., Tymianski, M., Crawley, A.P., Fisher, J.A., Mikulis, D.J., 2010. Steal physiology is spatially associated with cortical thinning. Journal of Neurology, Neurosurgery and Psychiatry 81, 290–293.
Fischl, B., Dale, A.M., 2000. Measuring the thickness of the human cerebral cortex from magnetic resonance images. Proceedings of the National Academy of Sciences of the United States of America 97, 11050–11055.
Fischl, B., Rajendran, N., Busa, E., Augustinack, J., Hinds, O., Yeo, B.T., Mohlberg, H., Amunts, K., Zilles, K., 2008. Cortical folding patterns and predicting cytoarchitecture. Cerebral Cortex 18, 1973–1980.
Fischl, B., Salat, D.H., van der Kouwe, A.J.W., Makris, N., Segonne, F., Quinn, B.T., Dale, A.M., 2004a. Sequence-independent segmentation of magnetic resonance images. Neuroimage 23, S69–S84.
Fischl, B., Sereno, M.I., Dale, A.M., 1999a. Cortical surface-based analysis. II: inflation, flattening, and a surface-based coordinate system. Neuroimage 9, 195–207.
Fischl, B., Sereno, M.I., Tootell, R.B., Dale, A.M., 1999b. High-resolution intersubject averaging and a coordinate system for the cortical surface. Human Brain Mapping 8, 272–284.
Fischl, B., van der Kouwe, A., Destrieux, C., Halgren, E., Segonne, F., Salat, D.H., Busa, E., Seidman, L.J., Goldstein, J., Kennedy, D., Carviness, V., Makris, N., Rosen, B., Dale, A.M., 2004b. Automatically parcellating the human cerebral cortex. Cerebral Cortex 14, 11–22.
Fjell, A.M., Westlye, L.T., Amlien, I., Espeseth, T., Reinvang, I., Raz, N., Agartz, I., Salat, D.H., Greve, D.N., Fischl, B., Dale, A.M., Walhovd, K.B., 2009. High consistency of regional cortical thinning in aging across multiple samples. Cerebral Cortex 19, 2001–2012.
Fleisher, A.S., Sherzai, A., Taylor, C., Laugbaum, J.B.S., Chen, K., Buxton, R.B., 2009. Resting-state BOLD networks versus task-associated functional MRI for distinguishing Alzheimer's disease risk groups. Neuroimage 47, 1678–1690.
Folstein, M.F., Folstein, S.E., McHugh, P.R., 1975. "Mini-mental state". A practical method for grading the cognitive state of patients for the clinician. Journal of Psychiatric Research 12, 189–198.
Forette, F., Seux, M.L., Staessen, J.A., Thijs, L., Babarskiene, M.R., Babeanu, S., Bossini, A., Fagard, R., Gil-Extremera, B., Laks, T., Kobalava, Z., Sarti, C., Tuomilehto, J., Vanhanen, H., Webster, J., Yodfat, Y., Birkenhager, W.H., Investigators, S.H.i.E., 2002. The prevention of dementia with antihypertensive treatment: new evidence from the Systolic Hypertension in Europe (Syst-Eur) study. Archives of Internal Medicine 162, 2046–2052.
Genovese, C.R., Lazar, N.A., Nichols, T., 2002. Thresholding of statistical maps in functional neuroimaging using the false discovery rate. Neuroimage 15, 870–878.
Girouard, H., Iadecola, C., 2006. Neurovascular coupling in the normal brain and in hypertension, stroke, and Alzheimer disease. Journal of Applied Physiology 100, 328–335.
Gjedde, A., Johannsen, P., Cold, G.E., Østergaard, L., 2005. Cerebral metabolic response to low blood flow: possible role of cytochrome oxidase inhibition. Journal of Cerebral Blood Flow and Metabolism 25, 1183–1196.
Greve, D.N., Fischl, B., 2009. Accurate and robust brain image alignment using boundary-based registration. Neuroimage 48, 68–72.
Grober, E., Silwinski, M., 1991. Development and validation of a model for estimating premorbid verbal intelligence in the elderly. Journal of Clinical and Experimental Neuropsychology 13, 933–949.
Gruhn, N., Larsen, F.S., Boesgaard, S., Knudsen, G.M., Mortensen, S.A., Thomsen, G., Aldershvile, J., 2001. Cerebral blood flow in patients with chronic heart failure before and after heart transplantation. Stroke 11, 2530–2533.
Gsell, W., De Sadeleer, C., Marchalant, Y., MacKenzie, E.T., Schumann, P., Dauphin, F., 2000. The use of cerebral blood flow as an index of neuronal activity in functional neuroimaging: experimental and pathophysiological considerations. Journal of Chemical Neuroanatomy 20, 215–224.
Hayasaka, S., Du, A.-T., Duarte, A., Kornak, J., Jahng, G.H., Weiner, M.W., Schuff, N., 2006. A non-parametric approach for co-analysis of multi-modal brain imaging data: application to Alzheimer's disease. Neuroimage 30, 768–779.
Helenius, J., Perkio, J., Soinne, L., Østergaard, L., Carano, R.A.D., Salonen, O., Savolainen, S., Kaste, M., Aronen, H.J., Tatlisumak, T., 2003. Cerebral hemodynamics in a healthy population measured by dynamic susceptibility contrast MR imaging. Acta Radiologica 44, 538–546.
Helzner, E.P., Luchsinger, J.A., Scarmeas, N., Cosentino, S., Brickman, A.M., Glymour, M.M., Stern, Y., 2009. Contribution of vascular risk factors to the progression in Alzheimer disease. Archives of Neurology 66, 343–348.
Heo, S., Prakash, R.S., Vossa, M., Erickson, K.I., Ouyang, C., Sutton, B.P., Kramer, A.F., 2010. Resting hippocampal blood flow, spatial memory and aging. Brain Research 1315, 119–127.
Hoge, R.D., Atkinson, J., Gill, B., Crelier, G.R., Marrett, S., Pike, G.B., 1999. Linear coupling between cerebral blood flow and oxygen consumption in activated human cortex. Proceedings of the National Academy of Sciences of the United States of America 96, 9403–9408.
Inoue, K., Ito, H., Goto, R., Nakagawa, M., Kinomura, S., Sato, T., Sato, K., Fukuda, H., 2005. Apparent CBF decrease with normal aging due to partial volume effects: MR-based partial volume correction on CBF SPECT. Annals of Nuclear Medicine 19, 283–290.
Inoue, K., Nakagawa, M., Goto, R., Kinomura, S., Sato, T., Sato, K., Fukuda, H., 2003. Regional differences between 99mTc-ECD and 99mTc-HMPAO SPET in perfusion changes with age and gender in healthy adults. European Journal of Nuclear Medicine and Molecular Imaging 30, 1489–1497.
Ishii, K., Sasaki, M., Kitagaki, H., Sakamoto, S., Yamaji, S., Maeda, K., 1996. Regional difference in cerebral blood flow and oxidative metabolism in human cortex. Journal of Nuclear Medicine 37, 1086–1088.
Ito, H., Inoue, K., Goto, R., Kinomura, S., Taki, Y., Okada, K., Sato, K., Sato, T., Kanno, I., Fukuda, H., 2006. Database of normal human cerebral blood flow measured by SPECT: I. Comparison between I-123-IMP, Tc-99m-HMPAO, and Tc-99m-ECD as referred with O-15 labeled water PET and voxel-based morphometry. Annals of Nuclear Medicine 20, 131–138.
Jiang, L., Kim, M., Chodkowski, B., Donahue, M.J., Pekar, J.J., Van Zijl, P.C.M., Albert, M., 2010. Reliability and reproducibility of perfusion MRI in cognitively normal subjects. Magnetic Resonance Imaging 28, 1283–1289.
Jones, K., Johnson, K.A., Becker, J.A., Spiers, P.A., Albert, M.S., Holman, B.L., 1998. Use of singular value decomposition to characterize age and gender differences in SPECT cerebral perfusion. Journal of Nuclear Medicine 39, 965–973.
Koehler, R.C., Roman, R.J., Harder, D.R., 2009. Astrocytes and the regulation of cerebral blood flow. Trends in Neurosciences 32, 160–169.
Law, I., Iida, H., Holm, S., Nour, S., Rostrup, E., Svarer, C., Paulson, O.B., 2000. Quantitation of regional cerebral blood flow corrected for partial volume effect using O-15 water and PET: II. Normal values and gray matter blood flow response to visual activation. Journal of Cerebral Blood Flow and Metabolism 20, 1252–1263.
Lee, C., Lopez, O.L., Becker, J.T., Raji, C., Dai, W., Kuller, L.H., Gach, H.M., 2009. Imaging cerebral blood flow in the cognitively normal aging brain with arterial spin labeling: implications for imaging of neurodegenerative disease. Journal of Neuroimaging 19, 344–352.
Leenders, K.L., Perani, D., Lammertsma, A.A., Heather, J.D., Buckingham, P., Healy, M.J.R., Gibbs, J.M., Wise, R.J.S., Hatazawa, J., Herold, S., Beaney, R.P., Brooks, D.J., Spinks, T., Rhodes, C., Frackowiak, R.S., Jones, T., 1990. Cerebral blood flow, blood volume and oxygen utilization. Brain 113, 24–47.
Li, Z.J., Matsuda, H., Asada, T., Ohnishi, T., Kanetaka, H., Imabayashi, E., Tanaka, F., 2004. Gender difference in brain perfusion 99mTc-ECD SPECT in aged healthy volunteers after correction for partial volume effects. Nuclear Medicine Communications 25, 999–1005.
Lu, H., Donahue, M.J., van Zijl, P.C.M., 2006. Detrimental effects of BOLD signal in arterial spin labeling fMRI at high field strength. Magnetic Resonance in Medicine 56, 546–552.
MacIntosh, B.J., Filippini, N., Chappell, M.A., Woolrich, M.W., Mackay, C.E., Jezzard, P., 2010. Assessment of arterial arrival times derived from multiple inversion time pulsed arterial spin labeling MRI. Magnetic Resonance in Medicine 63, 641–647.
Matsuda, H., Kanetaka, H., Ohnishi, T., Asada, T., Imabayashi, E., Nakano, S., Katoh, A., Tanaka, F., 2002. Brain SPET abnormalities in Alzheimer's disease before and after atrophy correction. European Journal of Nuclear Medicine and Molecular Imaging 29, 1502.
Matsuda, H., Ohnishi, T., Asada, T., Li, Z.J., Kanetaka, H., Imabayashi, E., Tanaka, F., Nakano, S., 2003. Correction for partial-volume effects on brain perfusion SPECT in healthy men. Journal of Nuclear Medicine 44, 1243–1252.
Meltzer, C.C., Cantwell, M.N., Greer, P.J., Ben-Eliezer, D., Smith, G., Frank, G., Kaye, W.H., Houck, P.R., Price, J.C., 2000. Does cerebral blood flow decline in healthy aging? A PET study with partial-volume correction. Journal of Nuclear Medicine 41, 1842–1848.

Meyer, J.S., Takashima, S., Terayama, Y., Obara, K., Muramatsu, K., Weathers, S., 1994. CT changes associated with normal aging of the human brain. Journal of the Neurological Sciences 123, 200–208.
Mitsumori, F., Watanabe, H., Takaya, N., 2009. Estimation of brain iron concentration in vivo using a linear relationship between regional iron and apparent transverse relaxation rate of tissue water at 4.7 T. Magnetic Resonance in Medicine 62, 1326–1330.
Morrison, J.H., Hof, P.R., 1997. Life and death of neurons in the aging brain. Science 278, 412–419.
Nagata, K., Maruya, H., Yuya, H., Terashi, H., Mito, Y., Kato, H., Sato, M., Satoh, Y., Watahiki, Y., Hirata, Y., Yokoyama, E., Hatazawa, J., 2000. Can PET data differentiate Alzheimer's disease from vascular dementia? Annals of the New York Academy of Sciences 903, 252–261.
Obara, K., Meyer, J.S., Motel, K.F., Muramatsu, K., 1994. Cognitive declines correlate with decreased cortical volume and perfusion in dementia of Alzheimer type. Journal of the Neurological Sciences 127, 96–102.
Oguz, K.K., Golay, X., Pizzini, F.B., Freer, C.A., Winrow, N., Ichord, R., Casella, J.F., Zijl, P.C.M.v., Melhem, E.R., 2003. Sickle cell disease: continuous arterial spin-labeling perfusion MR imaging in children. Radiology 227, 567–574.
Østergaard, L., Weisskoff, R.M., Chesler, D.A., Gyldensted, C., Rosen, B.R., 1996 High resolution measurement of cerebral blood flow using intravascular tracer bolus passages. Part I: mathematical approach and statistical analysis. Magnetic Resonance in Medicine 36 715–725.
Pagani, M., Salmaso, D., Jonsson, C., Hatherly, R., Jacobsson, H., Larsson, S.A., Wägner, A., 2002. Regional cerebral blood flow as assessed by principal component analysis and (99m)Tc-HMPAO SPET in healthy subjects at rest: normal distribution and effect of age and gender. European Journal of Nuclear Medicine and Molecular Imaging 29, 67–75.
Pantano, P., Baron, J.C., Lebrun-Grandié, P., Duquesnoy, N., Bousser, M.G., Comar, D., 1984. Regional cerebral blood flow and oxygen consumption in human aging. Stroke 15, 635–641.
Parkes, L.M., Rashid, W., Chard, D.T., Tofts, P.S., 2004. Normal cerebral perfusion measurements using arterial spin labelign: reproducibility, stability, and age and gender effects. Magnetic Resonance in Medicine 51, 736–743.
Qiu, M., Maguire, R.P., Arora, J., Planeta-Wilson, B., Weinsimmer, D., Wang, J., Wang, Y., Kim, H., Rajeevan, N., Huang, Y., Carson, R.E., Constable, R.T., 2010. Arterial transit time effects in pulsed arterial spin labeling CBF mapping: insight from a PET and MR study in normal human subjects. Magnetic Resonance in Medicine 63, 374–384.
Raichle, M.E., MacLeod, A.M., Snyder, A.Z., Powers, W.J., Gusnard, D.A., Shulman, G.L., 2001. A default mode of brain function. Proc. Natl. Acad. Sci. U. S. A 98, 676–682.
Raichle, M.E., Snyder, A.Z., 2007. A default mode of brain function: a brief history of an evolving idea. Neuroimage 37, 1083–1090.
Raz, N., Gunning, F.M., Head, D., Dupuis, J.H., McQuain, J., Briggs, S.D., Loken, W.J., Thornton, A.E., Acker, J.D., 1997. Selective aging of the human cerebral cortex observed in vivo: differential vulnerability of the prefrontal gray matter. Cerebral Cortex 7, 268–282.
Raz, N., Rodrigue, K.M., Kennedy, K.M., Head, D., Gunning-Dixon, F., Acker, J.D., 2003. Differential aging of the human striatum: longitudinal evidence. AJNR. American Journal of Neuroradiology 24, 1849–1856.
Rosas, H.D., Liu, A.K., Hersch, S., Glessner, M., Ferrante, R.J., Salat, D.H., van der Kouwe, A., Jenkins, B.G., Dale, A.M., Fischl, B., 2002. Regional and progressive thinning of the cortical ribbon in Huntington's disease. Neurology 58, 695–701.
Ruitenberg, A., den Heijer, T., Bakker, S.L., 2005. Cerebral hypoperfusion and clinical onset of dementia: the Rotterdam Study. Annals of Neurology 57, 789–794.
Sachdev, P.S., Brodaty, H., Looi, J.C., 1999. Vascular dementia: diagnosis, management and possible prevention. The Medical Journal of Australia 170, 81–85.
Salat, D.H., Buckner, R.L., Snyder, A.Z., Greve, D.N., Desikan, R.S., Busa, E., Morris, J.C., Dale, A.M., Fischl, B., 2004. Thinning of the cerebral cortex in aging. Cerebral Cortex 14, 721–730.
Salat, D.H., Lee, S.Y., van der Kouwe, A.J., Greve, D.N., Fischl, B., Rosas, H.D., 2009. Age-associated alterations in cortical gray and white matter signal intensity and grey to white matter contrast. NeuroImage 48, 21–28.
Schuff, N., Matsumoto, S., Kmiecik, J., Studholme, C., Du, A., Ezekiel, F., Miller, B.L., Kramer, J.H., Jagust, W.J., Chui, H.C., Weiner, M.W., 2009. Cerebral blood flow in ischemic vascular dementia and Alzheimer's disease, measured by arterial spin-labeling magnetic resonance imaging. Alzheimer's & Dementia 5, 454–462.
Segonne, F., Dale, A.M., Busa, E., Glessner, M., Salat, D., Hahn, H.K., Fischl, B., 2004. A hybrid approach to the skull stripping problem in MRI. Neuroimage 22, 1060–1075.
Segonne, F., Pacheco, J., Fischl, B., 2007. Geometrically accurate topology-correction of cortical surfaces using nonseparating loops. IEEE Trans. Med. Imag. 26, 518–529.
Shimizu, S., Zhang, Y., Laxamana, J., Miller, B.L., Kramer, J.H., Weiner, M.W., Schuff, N., 2010. Confordance and discordance between brain perfusion and atrophy in frontotemporal dementia. Brain Imaging Behav 4, 46–54.
Shin, W., Horowitz, S., Ragin, A., Chen, Y., Walker, M., Caroll, T.J., 2007. Quantitative cerebral perfusion using dynamic susceptibility contrast MRI: evaluation of reproducibility and age- and gender-dependence with fully automated image postprocessing algorithm. Magnetic Resonance in Medicine 58, 1232–1241.
Silva, A.C., Kim, S.G., 1999. Pseudo-continuous arterial spin labeling technique for measuring CBF dynamics with high temporal resolution. Magnetic Resonance in Medicine 42, 425–429.
Skoog, I., Lernfelt, B., Landahl, S., Palmertz, B., Andreasson, L.A., Nilsson, L., Persson, G., Odén, A., Svanborg, A., 1996. 15-year longitudinal study of blood pressure and dementia. Lancet 347, 1141–1145.
Sled, J.G., Zijdenbos, A.P., Evans, A.C., 1998. A nonparametric method for automatic correction of intensity nonuniformity in MRI data. IEEE Transactions on Medical Imaging 17, 87–97.
Sojkova, J., Beason-Held, L., Zhou, Y., An, Y., Kraut, M.A., Ye, W., Ferrucci, L., Mathis, C.A., Klunk, W.E., Wong, D.F., Resnick, S.M., 2008. Longitudinal cerebral blood flow and amyloid deposition: an emerging pattern? Journal of Nuclear Medicine 49, 1465–1471.
Sojkova, J., Najjar, S.S., Beason-Held, L., Metter, E.J., Davatzikos, C., Kraut, M.A., Zonderman, A.B., Resnick, S.M., 2010. Intima-media thickness and regional cerebral blood flow in older adults. Stroke 41, 273–279.
Sokoloff, L., Reivich, M., Kennedy, C., des Rosiers, M.H., Patlak, C.S., Pettigrew, K.D., Sakurada, O., Shinohara, M., 1977. The [^{14}C]deoxyglucose method for the measurement of local cerebral glucose utilization: theory, procedure, and normal values in the conscious and anesthetized albino rat. Journal of Neurochemistry 28, 897–916.
Sullivan, E.V., Rosenbloom, M., Serventi, K.L., A, P., 2004. Effects of age and sex on volumes of the thalamus, pons, and cortex. Neurobiology of Aging 25, 185–192.
Tohgi, H., Yonezawa, H., Takahashi, S., Sato, N., Kato, E., Kudo, M., Hatano, K., Sasaki, T., 1998. Cerebral blood flow and oxygen metabolism in senile dementia of Alzheimer's type and vascular dementia with deep white matter changes. Neuroradiol 40, 131–137.
Tosun, D., Mojabi, P., Weiner, M.W., Schuff, N., 2010. Joint analysis of structural and perfusion MRI for cognitive assessment and classification of Alzheimer's disease and normal aging. Neuroimage 52, 186–197.
Tzourio, C., Anderson, C., Chapman, N., Woodward, M., Neal, B., MacMahon, S., Chalmers, J., Group, P.C., 2003. Effects of blood pressure lowering with perindopril and indapamide therapy on dementia and cognitive decline in patients with cerebrovascular disease. Archives of Internal Medicine 163, 1069–1075.
Uh, J., Lewis-Amezcua, K., Martin-Cook, K., Cheng, Y., Weiner, M., Diaz-Arrastia, R., Devous Sr., M., Shen, D., Lu, H., 2010. Cerebral blood volume in Alzheimer's disease and correlation with tissue structural integrity. Neurobiology of Aging 31, 2038–2046.
van der Kouwe, A.J.W., Benner, T., Salat, D.H., Fischl, B., 2008. Brain morphometry with multiecho MPRAGE. Neuroimage 40, 559–569.
Van Laere, K.J., Dierckx, R.A., 2001. Brain perfusion SPECT: age- and sex-related effects correlated with voxel-based morphometric findings in healthy adults. Radiol 221, 810–817.
Vanderploeg, R.D., Schinka, J.A., Jones, T., Small, B.J., Graves, A.B., Mortimer, J.A., 2000. Elderly norms for the Hopkins Verbal Learning Test-Revised. The Clinical Neuropsychologist 14, 318–324.
Walhovd, K.B., Fjell, A.M., Reinvang, I., Lundervold, A., Dale, A.M., Eilertsen, D.E., Quinn, B.T., Salat, D.H., Makris, N., Fischl, B., 2005. Effects of age on volumes of cortex, white matter and subcortical strucutures. Neurobiology of Aging 26, 1261–1270.
Wang, J., Alsop, D.C., Li, L., Listerud, J., Gonzalez-At, J.B., Schnall, M.D., Detre, J.A., 2002. Comparison of quantitative perfusion imaging using arterial spin labeling at 1.5 and 4.0 Tesla. Magnetic Resonance in Medicine 48, 242–254.
Williams, D.S., Detre, J.A., Leigh, J.S., Koretsky, A.P., 1992. Magnetic resonance imaging of perfusion using spin inversion of arterial water. Proceedings of the National Academy of Sciences of the United States of America 89, 212–216.
Wong, E.C., Buxton, R.B., Frank, L.R., 1997. Implementation of quantitative perfusion imaging techniques for functional brain mapping using pulsed arterial spin labeling. NMR Biomed 10, 237–249.
Wong, E.C., Buxton, R.B., Frank, L.R., 1998a. Quantitative imaging of perfusion using a single subtraction (QUIPSS and QUIPSS II). Magnetic Resonance in Medicine 39, 702–708.
Wong, E.C., Buxton, R.B., Frank, L.R., 1998b. A theoretical and experimental comparison of continuous and pulsed arterial spin labeling techniques for quantitative perfusion imaging. Magnetic Resonance in Medicine 40, 348–355.
Wu, W.C., Edlow, B.L., Elliot, M.A., Wang, J., Detre, J.A., 2009. Physiological modulations in arterial spin labeling perfusion magnetic resonance imaging. IEEE Trans. Med. Imag. 28, 703–709.
Xu, G., Rowley, H.A., Wu, G., Alsop, D.C., Shankaranarayanan, A., Dowling, M., Christian, B.T., Oakes, T.R., Johnson, S.C., 2010. Reliability and precision of pseudo-continuous arterial-spin labeling perfusion MRI on 3.0 T and comparison with ^{15}O–water PET in elderly subjects at risk for Alzheimer's disease. NMR in Biomedicine 23, 286–293.
Yang, D.W., Kim, B.S., Park, J.K., Kim, S.Y., Kim, E.N., Sohn, H.S., 2002. Analysis of cerebral blood flow of subcortical vascular dementia with single photon emission computed tomography: adaptation of statistical parametric mapping. Journal of the Neurological Sciences 203–204, 199–205.
Ye, F.Q., Mattay, V.S., Jezzard, P., Frank, J.A., Weinberger, D.R., McLaughlin, A.C., 1997. Correction for vascular artifacts in cerebral blood flow values measured by using arterial spin tagging techniques. Magnetic Resonance in Medicine 37, 226–235.
Yesavage, J.A., Brink, T.L., Rose, T.L., Lum, O., Huang, V., Adey, M., Leirer, V.O., 1982. Development and validation of a geriatric depression screening scale: a preliminary report. Psychiatr Res 17, 37–49.
Zlokovic, B.V., 2005. Neurovascular mechanisms of Alzheimer's neurodegeneration. Trends in Neurosciences 28, 202–208.
Zollei, L., Stevens, A., Huber, K., Kakunoori, S., Fischl, B., 2010. Improved tractography alignment using combined volumetric and surface registration. Neuroimage 51, 206–213.
Zou, Q., Wu, C.W., Stein, E.A., Zang, Y., Yang, Y., 2009. Static and dynamic characteristics of cerebral blood flow during the resting state. Neuroimage 48, 515–524.